THE TECTONICS OF MERCURY: A POST MESSENGER VIEW. T. R. Watters[1], S. E. Anderson[1,2], [1]Center for Earth and Planetary Studies, National Air and Space Museum, Smithsonian Institution, Washington, DC 20560, USA (watterst@si.edu); [2]Aix Marseille Université, Marseille, FR.

Introduction: The MErcury Surface, Space ENvironment, GEochemistry, and Ranging (MESSENGER) mission after three flybys and over four years in orbit revolutionized our view of the innermost planet. MESSENGER revealed Mercury to be a planet with a truly remarkable tectonic story to tell. Orbital imaging campaigns with the Mercury Dual Imaging System (MDIS) wide-angle and narrow-angle cameras [1] provided global low-, moderate-, and high-incidence angle mosaics and targeted images. During the last 18 months of the mission, the spacecraft's periapsis altitude was lowered, providing the opportunity to image the surface at much higher spatial resolution [see 2]. The images and mosaics combined with topography from the Mercury Laser Altimeter (MLA) [3], stereo imaging [4, 5], and image-based control network techniques [6] have facilitated the production of regional and global maps for use in identifying and mapping tectonic landforms. Global mapping using high-incidence angle imaging (65° to 88°) with opposite solar azimuth directions and topography shows that Mercury's tectonic landforms can be divided into two spatially distinct classes, broadly distributed and basin-localized.

Broadly Distributed Tectonics: Contractional tectonic landforms are widely distributed on Mercury [7-13] and include lobate scarps, high-relief ridges, and wrinkle ridges. Of these, lobate scarps are the most broadly distributed (Fig. 1) and have the greatest range in scale with over 3 km of relief on the largest scarp [14] and only tens of meters of relief on the smallest [2]. These thrust fault scarps and the closely related, rarer high-relief ridges, are globally distributed, occuring dominantly in intercrater plains, having been active since the end of the late heavy bombardment (LHB) [15] and likely still forming [2]. The spatial distribution and areal density of the largest contractional landforms is not uniformly distributed, and the total length of mapped scarps is more than a factor of two greater in the southern hemisphere [13].

The most commonly cited model is global contraction which, absent other influences, would result in uniformly distributed population of randomly oriented lobate scarps [see 13]. It is clear from the distribution of orientations that global contraction alone cannot account for the spatial distribution and orientations of the lobate thrust fault scarps [13]. A combination of global contraction and tidal despinning can best account for the fault scarps [16-18]. The distribution of equatorial N-S and polar E-W oriented thrust fault scarps can be accounted for by extending equatorial thinning of the lithosphere poleward [17], consistent with the large latitudinal variation in surface temperatures [19], and avoids the need for an unrealistically weak brittle lithosphere (invoked by [18]). The observed transition from N-S to E-S thrust faults at about ±60° [13] suggests roughly equal contribution of stress from global contraction and tidal despinning [17]. This combination does not account for the nonuniform areal density of the contractional landforms (Fig. 1). Mantle convection is a plausible mechanism to concentrate faults. With Mercury's thin mantle, however, cells of comparable spatial scales to the distribution of fault scarps are problematic [20-24]. The distribution of faults correlates with regions of greater crustal thickness suggesting mantle downwelling might be a contributing mechanism [25, 26]. No single or combination of proposed models can fully account for both the spatial distribution and the orientations of the fault scarps.

Wrinkle ridges dominate Mercury's smooth plains that cover ~27% of the surface and are largely volcanic in origin [27-29]. The largest expanses are found in the northern high latitudes and exterior to the Caloris basin (Fig. 1). Mercury's ridged plains likely formed by stresses resulting from some combination of load-induced subsidence in response to thick accumulations of flood volcanic deposits and global contraction [10, 29]. Typical wrinkle ridges on Mercury have greater relief than their counterparts on the Moon [30] and far exceed lobate scarps and high-relief ridges in number.

Within many areas of volcanic plains encircled by rings of wrinkle ridges localized over the rims of buried impact structures are graben, commonly in polygonal patterns. These ridge-graben systems may result from a combination of thermal contraction of thick lava flow units and global contraction [31, 32].

Basin-localized Tectonics: Mercury's largest, well preserved impact basins Caloris and Rembrandt have complex arrangements of contractional and extensional tectonic landforms (Fig. 1). The interior volcanic plains of the Caloris have basin-concentric wrinkle ridges that extend to the center of the basin, and a system of basin-radial graben, Pantheon Fossae, radiating outward from the basin center, with some contributing to polygonal patterns near the basin margin [9, 33-35]. Rembrandt also has a complex arrangement of basin-radial and basin-concentric wrinkle ridges and graben that form a unique wheel-and-spoke-like pattern in its interior plains [36]. The pattern of ridges and graben in Rembrandt and Caloris is in stark contrast to those in lunar mascons where flexure and subsidence result in basin-interior wrinkle ridges and graben near and outside of basin-margins [see 37]. Unlike lunar mascons, inward lateral flow of the lower crust [11, 38] or loading by exterior volcanic plains [39, 40] contributed to the basin tectonics. Smaller basins, Raditladi, Rachmaninoff, and Mozart, have graben confined to smooth plains material interior to their

peak rings [9, 41]. Rachmaninoff and Mozart also have wrinkle ridges in their interior plains.

Mercury's Great Valley: The largest fault scarp on-Mercury, Enterprise Rupes, crosscuts the Rembrandt basin and a second scarp complex, Belgica Rupes, extends to the basin's rim. Stereo-derived topography shows that these tectonic landforms bound a broad, relatively flat-floored valley with a mean width of ~400 km [42]. The bounding fault scarps have opposite vergence, and the valley floor is significantly offset below the elevation of the back-scarp terrains. This offset and the localization of the widely spaced thrust faults suggests Mercury's great valley is the result of long-wavelength lithospheric buckling [42]. Topographic undulations that extent into the interior smooth plains of Caloris have wavelengths of up to 1300 km and amplitudes up to 3 km [35]. This scale far exceeds those expected from lithospheric buckling given the current estimates of Mercury's interior structure and thus they are likely not tectonic in origin [35]. Their association with positive gravity anomalies suggests support by deep-seated dynamic flow [26].

Radius Change: Some recent estimates of radius change expressed by Mercury's contractional landforms have reached epic levels. Estimates as high as 7 km have been reported [12] with speculation of even larger amounts due to putative unexpressed contractional strain [18]. Here tectonic landforms were mapped using a single polyline assigned to each landform to represent a primary fault. This is in contrast to other mapping efforts where multiple polylines are assigned to a single tectonic landform [12, 43] and weighted equally in assessments of contractional strain. The ratio γ of estimated maximum fault displacement to the measured fault length for lobate scarps and high-relief ridges is used to determine the total contractional strain [10, 11, 44]. Values of γ range from (~7.1–9.7) $\times 10^{-3}$ for values of the fault plane dip θ of 25° to 35°, with $\gamma \cong 8.2 \times 10^{-3}$ for $\theta = 30°$. For a given θ, the standard deviation of the slope (γ) is (~1.0–1.4) $\times 10^{-3}$. The areal contractional strain over the entire surface of the planet expressed by the mapped scarps is estimated to be ~0.063–0.096% (~0.08% for $\theta = 30°$). This range in contractional strain corresponds to a radius decrease of ~0.8–1.2 km (~1 km for $\theta = 30°$), consistent with previous estimates [10, 11, 44]. The wrinkle ridge dominated smooth plains likely resulted from some combination of load-induced flexure and subsidence and global contraction [10]. An estimate of the strain accommodated by global contraction alone may be obtained by eliminating the area covered by smooth plains. The areal contractional strain excluding lobate scarps within smooth plains is estimated to be ~0.08–0.12% (0.1% for $\theta = 30°$). This range in the contractional strain corresponds to a radius decrease of ~1–1.5 km (~1.2 km for $\theta = 30°$). The contribution of the small, young scarps to the radius change is relatively small due to their scale [2].

Long-lived, distributed thrust faulting, continuing to present day, and realistic estimates of radial contraction since the LHB are significant constraints to thermal history models. The discovery of a 3.9-Gyr-old remnant magnetic field poses a significant challenge to thermal history models that predict high rates of interior cooling [45]. The super contraction of Mercury, inferred post-LHB radius change >>2 km, is likely incompatible with thermal models that must account for Mercury's long-lived core dynamo and current contraction by slow cooling of the interior [2].

References: [1] Hawkins S.E., III, et al. (2007) *Space Sci. Rev.*, *131*, 247-338. [2] Watters T.R. et al. (2016) *Nature Geosci., 9*, 743-747. 2016 [3] Zuber M.T. et al. (2012) *Science*, *336*, 217-220. [4] Oberst J. et al. (2010) *Icarus 209*, 230-238. [5] Preusker F. et al. (2017) *PSS 142, 26-37*. [6] Becker, K.J. et al. (2016) *LPSC 47*, 2959. [7] Strom R.G., Trask N.J. and Guest J.E. (1975) *JGR, 80,* 2478-2507. [8] Watters T.R. et al. (2004) *GRL, 31*, L04701, 10.1029/2003GL019171. [9] Solomon S.C. et al. (2008) *Science, 321*, 59-62. [10] Watters T.R. et al. (2009) *Earth Planet. Sci. Lett.,* 285, 283–296. [11] Watters T.R. and Nimmo F. (2010) in *Planetary Tectonics*, Cambridge Univ. Press, 15-80. [12] Byrne P.K. et al. (2014) *Nature Geosci., 7*, 301-307. [13] Watters T.R. et al. (2015) *GRL, 42*, doi:10.1002/2015GL063570. [14] Watters T.R. et al. (2016) *GRL, 43*, 11536-11544. [15] Banks M.E. (2015) *JGR*, *120*, doi:10.1002/2015JE004828. [16] Dombard A.J. and Hauck S.A. (2008) *Icarus, 198*, 274–276. [17] Beuthe M. (2010) *Icarus 209*, 795–817. [18] Klimczak C. et al. (2015) *EPSL* 416, 82–90. [19] Williams, J.-P. et al. (2011) *JGR*, 116, doi:10.1029/2010JE003655. [20] King, S.D. (2008) *Nature Geosci., 1*, 229-232. [21] Smith D.E. (2012) *Science, 336*, 212-216 [22] Hauck, S.A. et al. (2013) *JGR*, *118*, 1204–1220. [23] Michel, N.C. et al. (2013) *JGR*, *118*, 1033–1044. [24] Tosi, N. et al. (2013) *JGR*, *118*, 2474–2487. [25] Selvans, M. M. et al. (2014) *LPSC 45*, 1442. [26] James, P.B. et al. (2015) *JGR*, *120*, 287–310. [27] Robinson M.A. (2008) *Science*, *321*, 66-69. [28] Denevi B.W. et al. (2009) *Science*, *324*, 613-618. [29] Head J.W. (2011) *Science*, *333*, 1853-1856, 2011. [30] Walsh, L.S. et al., (2013) *LPSC 44*, 2937. [31] Watters T.R. et al. (2012) *Geology, 40*, 1123-1126. [32] Klimczak C. et al. (2012) *JGR, 117*, doi:10.1029/2012JE004100. [33] Murchie S.L. et al. (2008) *Science*, *321*, 73-76. [34] Watters T.R. et al. (2009) *Earth Planet. Sci. Lett., 285*, 309-319. [35] Klimczak C. et al. (2013) *JGR*, *118*, 2030-2044. [36] Watters T.R. et al. (2009) *Science, 324*, 618-621. [37] Watters T.R. and Johnson (2010) in *Planetary Tectonics*, Cambridge Univ. Press, 121-182. [38] Watters T.R., Nimmo F. and Robinson M.S. (2005) *Geology, 33*, 669-672. [39] Melosh H.J. and McKinnon W.B. (1988) in *Mercury*, Univ. Arizona Press, Tucson, 374-400. [40] Kennedy, P.J., Freed, A.M. and Solomon, S.C. (2008) *JGR, 113*, 10.1029/2007JE002992. [41] Prockter L.M. et al. (2010) *Science*, *329*, 668-671, 2010. [42] Watters T.R. et al. (2016) *GRL, 43*, 11536-11544. [43] DiAchille, G., et al. (2012) *Icarus, 221,* 456-460. [44] Watters, T.R., et al. (1998) *Geology, 26,* 991-994. [45] Johnson, C.L. et al. (2015) *Science, 348*, 892-895.

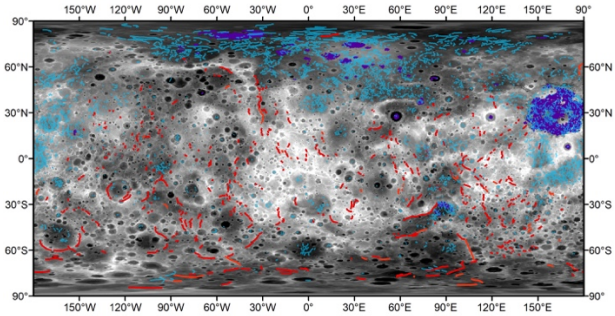

Figure 1. Tectonic landform on Mercury with lobate scarps and high-relief ridges (red), wrinkle ridges (blue) and graben (purple). Topography is shown in shades of grey, black (lowThe) and white (high) [6].